# $\alpha$-$d$ resonances and the low-lying states of $^6$Li

A. Eskandarian* and I. R. Afnan
*School of Physical Sciences, The Flinders University of South Australia, Bedford Park, South Australia 5042, Australia*
(Received 27 May 1992)

The low-lying states (below the $^3$He-$^3$H threshold) of the $^6$Li nucleus are generated using three-body models with two-body nonlocal separable interactions between the constituent particles. The positions and widths of the states are determined by searching for the eigenvalues of the kernel of the Faddeev equations in the complex energy plane. When appropriate (for $T = 0$ states only), the results are compared with a separate determination of these quantities from the $\alpha$-$d$ scattering process. All experimentally observed levels are found. Given that the Coulomb interaction is not included in our calculations, agreement with experiment is favorable for both the positions and the widths of the resonances.
PACS number(s): 21.60.Gx, 24.30.Gd, 27.20.+n

## I. INTRODUCTION

It is by now a well-established fact that at low excitation energies ($\lesssim$15 MeV) many properties of the $A = 6$ nuclei can be satisfactorily explained within the framework of three-body models. In these models the three constituents that make up the nucleus are an alpha particle and two nucleons. In the past two decades many successful calculations with three-body models based on nonlocal separable interactions between the constituent particles have been performed, e.g., elastic and inelastic $\alpha$-$d$ scattering [1–5], $^6$Li$\rightarrow \alpha + d$ momentum distribution [6, 7], $^6$Li$\rightarrow \alpha + d$ asymptotic normalization constants [6, 8], the $^6$Li$\rightarrow p + (n\alpha)$ spectral function [9], and $^6$He $\beta$ decay [10]. These three-body models are unambiguous in their dynamics and do not suffer from the center-of-mass problem which is associated with the harmonic-oscillator shell-model states. Moreover, no free parameters exist at the three-body level once the parameters of the underlying two-body interactions are determined.

In the context of three-body models and nonlocal separable interactions, Shanley's work on the elastic $\alpha$-$d$ scattering was the first of its kind in which the $^6$Li levels were produced from the behavior of the phase shifts obtained from the amplitudes [1]. Shanley included different $D$-state probabilities in the $NN$ interaction in order to assess the effect of the tensor force on his results. He also used a purely repulsive $N\alpha$ interaction in the $S_{1/2}$ channel. Given that the Coulomb interaction was not included, the binding energy was under bound by $\sim$0.3 MeV. This shortcoming was attributed to the uncertainties in the $N\alpha$ interaction [1]. The widths of the levels were not calculated in Shanley's paper. On the other hand, Koike's calculation [3], which utilized a better parametrization of the $N\alpha$ interaction, also reproduced the low-lying levels of $^6$Li from the behavior of the phase shifts, with remarkable improvement on Shanley's results. Here again, the focus of the work was not on the characteristics of the energy levels, thus the widths for those levels were not calculated. A specific calculation of the three-body resonances in $^6$Li was provided by Matsui who, for the bound states, solved the eigenvalue problem using the Schrödinger equation, and for the resonances, solved the complex eigenvalue problem for the Faddeev-type equations [11]. Unfortunately, Matsui's determination of the widths was only valid for resonances that lie close to the real energy axis. None of the above authors included the Coulomb interaction in their calculations.

The bound-state solutions of the Schrödinger equation for the $^6$Li and $^6$He nuclei, in the context of three-body models and nonlocal separable interactions, have been extensively studied by Lehman, Rai, and Ghovanlou [12] and by Ghovanlou and Lehman [13]. Their papers contain a comprehensive study of the role that different two-body interactions play for the bound state case. For example, the role of the tensor force in the $NN$, and the repulsive $S_{1/2}$ interaction in the $N\alpha$ subsystems were thoroughly delineated. Furthermore, in a separate paper, Lehman studied the effect of different representations of the $N\alpha$ interaction in the $S_{1/2}$ channel on the three-body binding energies of $^6$Li and $^6$He [14]. The $N\alpha$ interaction in the $S_{1/2}$ channel can be represented by either a repulsive potential or an attractive potential that will support a spurious bound state in the $N\alpha$ system. It is possible to exclude this spurious bound state from the attractive $S_{1/2}$ part of the $N\alpha$ interaction by a projection method [14, 15]. The behavior of the $N\alpha$ phase shifts at higher energies seems to indicate that it is preferable to represent the $S_{1/2}$ part of the $N\alpha$ interaction by an attractive potential. If one allows for an approximate correction due to the Coulomb interaction that was neglected in their calculations, in the models

*Present address: Physics Department, George Washington University, Washington, D.C. 20052.

 

that faithfully take into account the physics of the underlying two-body interactions, the results obtained by Lehman and collaborators [12–14] are in very good agreement with experiment.

The encouraging work of the above authors shows that, as mentioned before, the $A = 6$ nuclei can be satisfactorily treated within the context of three-body models for low excitation energies. Our aim in undertaking the following calculations is to complete the existing theoretical understanding of the $^6$Li nucleus by providing an unambiguous level diagram for the low-lying states of $^6$Li in which the widths as well as the positions of these levels are calculated to the best of our present computational ability. Our calculation differs from the previous attempts in that the widths of the resonances are obtained simultaneously with the solution to the homogeneous Faddeev-type integral equations, and without any approximations. We can then compare these results (for the $T = 0$ states only) with a calculation from the $\alpha$-$d$ scattering amplitudes. The three-body resonances should be the same in both calculations. The two-body threshold effects, however, are present in the $\alpha$-$d$ scattering problem to the extent that they can result in resonance-type behavior in the observed amplitudes [16, 17]. If a three-body resonance is nearby, and depending on the widths of the resonances involved, it can be washed out by the effect of the two-body threshold. In this case, the experimentally observed bump in the $\alpha$-$d$ elastic scattering is really the effect of the two-body threshold. The nearby three-body resonance then should be detected via a different process. These points will be discussed in more detail in the following sections.

In Sec. II we show first how a resonance state may be treated on equal footing with a bound state by examining the eigenvalues of the kernel of the integral equation for the $T$ matrix. We then present a brief derivation of the three-body equations for the $\alpha NN$ system including the antisymmetrization. Finally, we present the two-body amplitudes required for the solution of the three-body equations. Section III is devoted to the presentation of the results. Here we describe the method of contour rotation as applied to the $\alpha NN$ system. In particular, we discuss the analytic continuation of the three-body equations to the energy domain where the resonance poles reside. To illustrate any difference between the extraction of resonance parameters from the experimental data with the results of searches for the poles of the $S$ matrix, we compare the speed analysis on the $\alpha$-$d$ amplitude in this model with the results of the search for the poles of the scattering amplitude on the second Riemann sheet of the energy plane. Finally, in Sec. IV we state our conclusions.

## II. FORMALISM

To establish the relation between the experimental scattering data and the theoretical definition of a resonance, we commence this section by a general discussion of what we mean by a resonance and how it manifests itself in the experimental cross section. Since the system we are considering is modeled in terms of three-particle equations, we present the corresponding eigenvalue problem we have to solve to get the bound and resonance states for the $\alpha NN$ system, and for completeness we give the corresponding equations that give us the scattering amplitude for $\alpha$-$d$ scattering. To examine the sensitivity of our results to the input two-body amplitudes, we present the two-body $\alpha N$ and $NN$ separable potentials used in our analysis.

### A. Definition of resonances

Experimentally, we often observe structures in the energy dependence of cross sections, which we refer to as resonances. With sufficient experimental data, we can perform a phase shift analysis from which we can examine the energy dependence of the individual partial waves amplitudes. Here the simplest analysis involves an Argand plot which gives the plot of the imaginary part of the scattering amplitude versus the real part as the energy varies. A counterclockwise loop in the Argand diagram is often considered a signature for a resonance. A more stringent test for the determination of the existence of a resonance is a speed plot [18]. Here, we examine the energy dependence of the magnitude of the energy derivative of the scattering amplitude, i.e., $|\frac{dT_\ell}{dE}|$. In this way we eliminate the energy independent background amplitude, and what is left is the contribution from the resonant amplitude. If this resonance amplitude corresponds to a simple pole on the fourth quadrant of the energy sheet, then a speed plot would give us a Breit-Wigner form, from which we can extract the position of the pole of the scattering amplitude in the complex energy plane, i.e., $E_R$. In other words, we can determine the position of the resonance ($\mathrm{Re}[E_R]$) and the width of the resonance ($\mathrm{Im}[E_R]$). This procedure for the analysis of the experimental data basically assumes that the scattering amplitude in a given partial wave is the sum of an energy independent background term plus an energy dependent resonance term, with the latter represented by a simple pole in the complex energy plane. In the above analysis it is assumed that there is a one to one correspondence between the poles of the scattering amplitude and the energies of bound and scattering states.

It is well known that at energies above the threshold for inelastic scattering we can get resonance effects due to the rapid opening of an inelastic channel. In this case the simple description of the energy dependence of the partial wave amplitude just in terms of a pole in the complex energy plane is wrong, as the threshold for inelastic scattering introduces a branch point into the analytic structure of the scattering amplitude [16, 17]. This branch point can give rise to rapid energy variation in more than one partial wave, and to that extent may not be considered as a resonance. To take this branch point into consideration in the analysis of the data requires that we employ a set of coupled equations which build in the threshold. But now the problem is that the analysis of the data is by no means simple, and is often not unique as we do not know the strength of the branch point [17]. In summary, the ultimate aim of the experimental analysis is to take all of the data and construct an analytic continuation of the

scattering amplitude into the complex energy plane so as to determine the position of the poles in the scattering amplitude that give rise to rapid variation in the cross section.

The main interest in determining these poles is that they are eigenstates of the Hamiltonian, and to that extent any information we have about the resonance states is as important as the information we have about the bound states of the system. We should therefore try to determine both the energy and wave function for the resonance. In the case of the $A = 6$ system, the energies of the resonances will give us the low energy spectrum of $^6$Li and $^6$He as well as the width of each state, while the wave function can be used to calculate other properties of these states, such as electromagnetic moments. In this section we will demonstrate first how the resonances are eigenstates of the Hamiltonian, and how we propose to solve the corresponding equations to determine these eigenstates.

We first consider a simple two-body system described by the Schrödinger equation, i.e.,

$$H\,|\psi\rangle = E\,|\psi\rangle \ . \tag{1}$$

Since the Hamiltonian $H$ is in general Hermitian, the eigenvalue problem in Eq. (1) has solutions only for real values of $E$. This automatically excludes resonances as eigenvalues of the Hamiltonian as predicted by Eq. (1). In fact, this result suggests that if we define the above equation in the complex energy plane, the only solutions we have are on the real axis. Clearly, to get the resonance solutions we need to analytically continue this equation onto the second Riemann sheet of the complex energy plane. This can be achieved in coordinate space by the method of dilatation group transformation [19–21], which renders a Hamiltonian that is complex, and admits complex eigenvalues. On the other hand, in the momentum representation we follow the procedure suggested by Lovelace [22] of first converting the differential equation in Eq. (1) into an integral equation of the form

$$|\psi\rangle = G_0(E)\,V\,|\psi\rangle \ , \tag{2}$$

where $V$ is the two-body interaction and the free Green's function $G_0(E) = (E - H_0)^{-1}$ with $H_0 = H - V$ being the kinetic energy operator, and then by rotating the contour of integration to expose that part of the complex energy plane where the resonances reside. By a simple analysis we can show that the two methods are identical [23] and there is a one to one correspondence between the angle of rotation in momentum space, and the parameter of the dilatation group transformation. This procedure, in either coordinate or momentum space, essentially extends the energy domain over which the Schrödinger equation or Lippmann-Schwinger equation is defined. Furthermore, the eigenstates in this new energy domain are normalizable [23].

To establish the fact that there is a one to one correspondence between the solution of Eq. (2) and the poles of the $T$ matrix, we consider, for the two-body case, the Lippmann-Schwinger equation for the $T$ matrix, which is given by

$$T_\ell(E) = V_\ell + V_\ell\,G_0(E)\,T_\ell(E) \ , \tag{3}$$

where $\ell$ labels the partial wave under consideration. The solution of this equation can be written in terms of the solution of the corresponding homogeneous eigenvalue equation, i.e.,

$$\lambda_n(E)\,|\phi_\ell^{(n)}\rangle = V_\ell\,G_0(E)\,|\phi_\ell^{(n)}\rangle \ , \tag{4}$$

as [23]

$$T_\ell(E) = \sum_n \frac{|\phi_\ell^{(n)}\rangle\langle\tilde{\phi}_\ell^{(n)}|\,V}{1-\lambda_n(E)} \ , \tag{5}$$

where $\langle\tilde{\phi}_\ell^{(n)}|$ is the eigenstate of the adjoint kernel. It is clear from the result of Eq. (5) that for any energy for which the eigenvalue $\lambda_n = 1$, the $T$ matrix has a pole. Bound states will correspond to real negative energies on the first Riemann sheet where $\lambda_n = 1$, while resonances correspond to energies in the fourth quadrant and near the real axis of the second Riemann sheet where $\lambda_n(E) = 1$. Thus to find the bound and resonance states of the system we have to find the energies at which one of the eigenvalues of the homogeneous Lippmann-Schwinger equation is one. Since the homogeneous Lippmann-Schwinger equation is identical to Eq. (2) with the substitution $|\psi\rangle = G_0(E)\,|\phi\rangle$, we have established the fact that the solution of the Schrödinger equation for a bound or resonance state is identical to the determination of the energy for which the kernel of the Lippmann-Schwinger equation has an eigenvalue $\lambda_n(E) = 1$. Although the above result was derived for the two-body system, the extension to the three-body system involves the replacement of the Lippmann-Schwinger equation by either the Faddeev-Lovelace equation or the Alt-Grassberger-Sandhas (AGS) equations [24], i.e., to determine the bound and resonance states of a three-body problem we need to find those energies at which the kernel of the AGS equations has an eigenvalue of one. In the next section we will consider the AGS equation for the $\alpha NN$ system when the two-body interaction is separable, and define the kernel whose eigenvalues we need to determine. In this case the method of rotation of contour, to extend the energy domain to include resonance energies, is more complicated than was the case for the corresponding two-body system because of the singularities of the three-body kernel. We will be discussing these singularities and the limitation they impose on the angle of rotation in the section on numerical results.

### B. Three-body equations

The AGS-type integral equations that properly describe the elastic $\alpha$-$d$ scattering and at the same time yield the bound states and resonances of the $\alpha NN$ system, have been derived many times in the literature [1, 3]. To be more definite, we briefly elaborate on the equations we have used and explain the nomenclature. In the derivation of the three-body equations one usually starts from the Alt, Grassberger, and Sandhas (AGS) equations [24] for the three-body scattering amplitude, $U_{\alpha\beta}$,

that describes the reaction $\alpha + (\beta\gamma) \leftarrow \beta + (\gamma\alpha)$, i.e.,

$$U_{\alpha\beta}(E) = \bar{\delta}_{\alpha\beta}\, G_0^{-1}(E) + \sum_{\gamma} \bar{\delta}_{\alpha\gamma}\, T_\gamma(E)\, G_0(E)\, U_{\gamma\beta}(E) \,. \tag{6}$$

Here $\bar{\delta}_{\alpha\beta} = 1 - \delta_{\alpha\beta}$, and the three-body free Green's function, $G_0(E)$, is given by

$$G_0(E) = (E - H_0)^{-1} \,, \tag{7}$$

where $H_0$, the Hamiltonian for the three noninteracting particles, is given by

$$H_0 = \sum_{i=1}^{3} \frac{k_i^2}{2m_i} = \frac{p_\alpha^2}{2\nu_\alpha} + \frac{q_\alpha^2}{2\mu_\alpha} \,. \tag{8}$$

In Eq. (8), $\mathbf{k_i}$ are the momenta of the three particles in the center of mass, and $m_i$ are the masses of the individual constituent particles; $\mathbf{p}_\alpha$ is the conjugate Jacobi coordinate (Jacobi momentum) designating the relative momentum of the $(\beta\gamma)$ pair of particles; $\mathbf{q}_\alpha$ is the Jacobi momentum designating the momentum of the particle labeled by $\alpha$ relative to the $(\beta\gamma)$ pair. The reduced masses $\nu_\alpha$ and $\mu_\alpha$ and the Jacobi momenta $\mathbf{p}_\alpha$ and $\mathbf{q}_\alpha$ can be expressed in terms of $\mathbf{k_i}$ and $m_i$ as follows:

$$\mathbf{p}_\alpha = \frac{\mathbf{m}_\gamma \mathbf{k}_\beta - \mathbf{m}_\beta \mathbf{k}_\gamma}{\mathbf{m}_\gamma + \mathbf{m}_\beta} \,, \tag{9}$$

$$\mathbf{q}_\alpha = \frac{\mathbf{m}_\alpha(\mathbf{k}_\beta + \mathbf{k}_\gamma) - (\mathbf{m}_\beta + \mathbf{m}_\gamma)\mathbf{k}_\alpha}{\mathbf{m}_\alpha + \mathbf{m}_\beta + \mathbf{m}_\gamma}$$

and

$$\nu_\alpha = \frac{m_\beta m_\gamma}{m_\beta + m_\gamma} \,, \quad \mu_\alpha = \frac{m_\alpha(m_\beta + m_\gamma)}{m_\alpha + m_\beta + m_\gamma} \,. \tag{10}$$

We can write the AGS equations as a set of coupled one-dimensional integral equations by introducing separable two-body amplitudes, in the three-body Hilbert space, for both the $NN$ and $N\alpha$ interactions. The derivation is standard and after a few steps, and remembering that the total angular momentum and isospin are conserved, one gets a set of coupled equations for the partial-wave amplitudes which are of the form [25]

$$\mathbf{X}^{J^\pi T}_{K_\alpha;K_\beta}(q_\alpha, q_\beta; E^+) = \mathbf{Z}^{J^\pi T}_{K_\alpha;K_\beta}(q_\alpha, q_\beta; E^+) + \sum_{K_\gamma} \int_0^\infty dq_\gamma\, q_\gamma^2\, \mathbf{Z}^{J^\pi T}_{K_\alpha;K_\gamma}(q_\alpha, q_\gamma; E^+) \tau_{n_\gamma}(E^+ - \varepsilon_\gamma(q_\gamma))\, \mathbf{X}^{J^\pi T}_{K_\gamma;K_\beta}(q_\gamma, q_\beta; E^+) \,. \tag{11}$$

In the above equation $\varepsilon_\gamma(q_\gamma) = \frac{q_\gamma^2}{2\mu_\gamma}$, and $K_\alpha = \{t_\alpha, j_\alpha, S_\alpha, \mathcal{S}_\alpha, \mathcal{L}_\alpha\}$ are the quantum numbers that label the different three-body channels for a given total angular momentum $J$, parity $\pi$, and isospin $T$. The following angular momentum and isospin coupling scheme is used:

$$\begin{aligned} &\mathbf{S}_\alpha = \mathbf{s}_\beta + \mathbf{s}_\gamma \,, \quad \mathbf{j}_\alpha = \boldsymbol{\ell}_\alpha + \mathbf{S}_\alpha \,, \quad \mathbf{t}_\alpha = \boldsymbol{\tau}_\beta + \boldsymbol{\tau}_\gamma, \\ &\boldsymbol{\mathcal{S}}_\alpha = \mathbf{j}_\alpha + \mathbf{s}_\alpha \,, \quad \mathbf{J} = \boldsymbol{\mathcal{L}}_\alpha + \boldsymbol{\mathcal{S}}_\alpha \,, \quad \mathbf{T} = \mathbf{t}_\alpha + \boldsymbol{\tau}_\alpha. \end{aligned} \tag{12}$$

Here, $\mathbf{s}_\beta$ and $\boldsymbol{\tau}_\beta$ refer to the spin and isospin of the particle labeled by $\beta$, $\boldsymbol{\ell}_\alpha$ refers to the relative orbital angular momentum of the $(\beta\gamma)$ pair, $\boldsymbol{\mathcal{S}}_\alpha$ is the channel spin; and $\boldsymbol{\mathcal{L}}_\alpha$ is the orbital angular momentum of the spectator particle $\alpha$ relative to the $(\beta\gamma)$ pair. With these specifications, $n_\gamma$ in Eq. (11) refers to the quantum numbers of the two-body subsystem for which particle $\gamma$ is the spectator, i.e., $n_\gamma = \{t_\gamma, j_\gamma, S_\gamma\}$. The Born term is given as the matrix element of the free three-particle Green's function, i.e. [25],

$$\mathbf{Z}^{J^\pi T}_{K_\alpha;K_\beta}(q_\alpha, q_\beta; E^+) = \bar{\delta}_{\alpha\beta}\, \langle \mathbf{g}_{n_\alpha};\, q_\alpha\, K_\alpha\, JT |\, G_0(E^+)\, | \mathbf{g}_{n_\beta};\, q_\beta\, K_\beta\, JT \rangle \,, \tag{13}$$

where $\mathbf{g}_{n_\alpha}$ is the form factor of the separable potential in the $n_\alpha$ channel and will be discussed in more detail in the next section.

The bound, excited, and resonances states of the $(\alpha NN)$ system are described by the homogeneous part of the same integral equation that describes the $\alpha + d$ scattering process. In that process the possible final-state three-body channels are

$$\begin{aligned} &\alpha + (NN) \rightarrow \alpha + (NN) \\ &\qquad \rightarrow N + (N\alpha) \,. \end{aligned} \tag{14}$$

We immediately notice that because of the symmetry of the two nucleons, we may reduce the number of equations involved by antisymmetrizing with respect to the exchange of the nucleons [26, 27]. Let us designate the $\alpha + (NN)$ and $N + (N\alpha)$ channels by the subscripts "$i$" and "$f$," respectively. The final antisymmetrized amplitudes can then be symbolically written in a matrix equation as

$$\begin{pmatrix} \mathbf{X}_{i,i} \\ \mathbf{X}_{f,i} \end{pmatrix} = \begin{pmatrix} 0 \\ \mathbf{Z}_{f,i} \end{pmatrix} + \begin{pmatrix} 0 & \mathbf{Z}_{i,f} \\ \mathbf{Z}_{f,i} & \mathbf{Z}_{f,f} \end{pmatrix} \begin{pmatrix} \boldsymbol{\tau}_i & 0 \\ 0 & \boldsymbol{\tau}_f \end{pmatrix} \begin{pmatrix} \mathbf{X}_{i,i} \\ \mathbf{X}_{f,i} \end{pmatrix} \,. \tag{15}$$

From the properties of Eq. (13) it can be shown that

$\mathbf{Z}_{f,i} = \mathbf{Z}_{i,f}$. The kernel in the above equations can also be symbolically written as

$$K = \begin{pmatrix} 0 & \mathbf{Z}_{i,f} \\ \mathbf{Z}_{f,i} & \mathbf{Z}_{f,f} \end{pmatrix} \begin{pmatrix} \boldsymbol{\tau}_i & 0 \\ 0 & \boldsymbol{\tau}_f \end{pmatrix} . \tag{16}$$

All the general remarks made in the previous section on resonances also apply to this kernel. Our primary objective is to study the behavior of the eigenvalues of the above kernel in the complex energy plane and from that to extract the bound and the resonances states of our system. Moreover, by solving the inhomogeneous integral equation for the $\alpha$-$d$ scattering amplitude, we will be able to compare the resonance parameters extracted from the scattering amplitude at real positive energies with those extracted from the eigenvalue search. In this way we can determine the effect of the inelastic thresholds on the energy dependence of the cross section, and in turn will be able to put a confidence level on the resonance parameters extracted from experimental data.

### C. Two-body interactions

We mentioned earlier that assuming separable interactions in all the two-body subsystems enables one to reduce the AGS equations to a set of coupled one-dimensional integral equations. In this section we describe our choices for the separable interactions between the $(N\alpha)$ and $(NN)$ pairs.

First, we partial-wave expand our two-body potential in momentum space as

$$\langle \mathbf{p}\,|V|\mathbf{p}'\rangle = \sum_{n\ell\ell'} \langle \hat{p}|n\ell\rangle\, V^n_{\ell\ell'}(p,p')\, \langle n\ell'|\hat{p}'\rangle \ , \tag{17}$$

where $n = \{t, j, S\}$ stands for the total isospin $t$, total angular momentum $j$, and total spin $S$ of the two-body system (notice that for simplicity we have dropped the subscripts $\alpha, \beta$, and $\gamma$). For separable potentials in momentum space we can write

$$\begin{aligned} V^n_{\ell\ell'} &= g_{n\ell}(p)\, C^n_{\ell\ell'}\, g_{n\ell'}(p') \\ &= \langle p|g_{n\ell}\rangle\, C^n_{\ell\ell'}\, \langle g_{n\ell'}|p'\rangle \ , \end{aligned} \tag{18}$$

where $C^n_{\ell\ell'}$ are the strength parameters of the potentials. Since we are dealing with coupled channels for $\ell \neq \ell'$, we can write the above potential in matrix form as

$$\mathbf{V}_n(p,p') = \langle p|\mathbf{V}|p'\rangle \ , \tag{19}$$

where

$$\mathbf{V} = |\mathbf{g}_n\rangle\, \mathbf{C}_n\, \langle \mathbf{g}_n| \ , \tag{20}$$

and

$$[\mathbf{C}_n]_{\ell\ell'} = C^n_{\ell\ell'} \ , \qquad [|\mathbf{g}_n\rangle]_{\ell\ell'} = \delta_{\ell\ell'}\, |g_{n\ell}\rangle \ . \tag{21}$$

This potential includes the coupling due to the tensor force by admitting $C^n_{ll'} \neq 0$ for $\ell \neq \ell'$ . The corresponding scattering amplitude has the same partial-wave expansion as given in Eq. (17) with $\mathbf{t}_n(p,p',E)$ replacing $\mathbf{V}_n(p,p')$, and $\mathbf{t}_n(E)$ given by

$$\mathbf{t}_n(E) = |\mathbf{g}_n\rangle\, \boldsymbol{\tau}_n(E)\, \langle \mathbf{g}_n| \ , \tag{22}$$

with the two-body propagator given by

$$\begin{aligned} [\boldsymbol{\tau}_n]^{-1}(E) &= \left[\mathbf{C}_n^{-1} - \mathbf{G}_0(E)\right]^{-1} \\ &= \mathbf{C}_n\, \left[\mathbf{I} - \mathbf{G}_0(E)\, \mathbf{C}_n\right]^{-1} \ , \end{aligned} \tag{23}$$

where

$$\begin{aligned} [\mathbf{G}_0(E)]_{\ell\ell'} &= [\, \langle \mathbf{g}|\, \mathbf{G}_0(E)\, |\mathbf{g}\rangle\, ]_{\ell\ell'} \\ &= \delta_{\ell\ell'}\, \langle g_{n\ell}|\, G_\ell(E)\, |g_{n\ell}\rangle \ . \end{aligned} \tag{24}$$

In the above equations, $\mathbf{G}_0(E)$ designates (symbolically) the free Green's function in the two-body subspace and

$$\langle p|G_\ell(E)|p\rangle = \begin{cases} \left(E - \dfrac{p^2}{2\mu_{NN}}\right)^{-1} & \text{for } NN \text{ system} \ , \\ \left(E - \dfrac{p^2}{2\mu_{N\alpha}}\right)^{-1} & \text{for } N\alpha \text{ system} \ , \end{cases} \tag{25}$$

with $\mu_{NN}$ and $\mu_{N\alpha}$ being the reduced masses of the $NN$ and $N\alpha$ systems, respectively. Here we remind the reader that when dealing with quantities in the three-body Hilbert space (as in the last section), $\mu_{NN}$ and $\mu_{N\alpha}$ are referred to as $\nu_\alpha$'s with $\alpha$ designating the label for the appropriate spectator particle. Our choices for $g_{n\ell}(p)$, the form factors of the separable potentials, are as follows:

$$g_{n\ell}(p) = \frac{p^\ell}{[p^2 + \beta^2_{\ell j}]^{(\ell+2)/2}} \ , \quad \text{for the } NN \text{ interaction} \ ; \tag{26}$$

and

$$g_{n\ell}(p) = \frac{p^\ell}{[p^2 + \beta^2_{\ell j}]^{(\ell+1)}} \ , \quad \text{for the } N\alpha \text{ interaction} \ . \tag{27}$$

Here, $\beta_{\ell j}$ are the inverse range parameters of the potential; their values are tabulated, along with the strength parameters $(C^n_{\ell\ell'})$, in Tables I and II for the $NN$ and $N\alpha$ interaction, respectively. The virtues of the above two-body interactions are discussed extensively in the works of Lehman and co-workers [12, 13]. (We warn the readers that the strength parameters in Tables I and II are defined differently than those in the references just mentioned, but are consistent with the definition of the potential as given above.) We are now in a position to elaborate on the three-body models that are used in our calculations and have their bases in the parametrizations of our two-body interactions.

For $T = 0$ states of $^6$Li, the two-body $NN$ interaction (see Table I) is fitted to the low-energy properties of the deuteron and can be included with different values of the percentage $D$ state thus enabling us to assess the role of the tensor force in our calculations. For $T = 1$ states, the $NN$ interaction is in a spin singlet and the parameters of the interaction are fitted to the singlet ef-

TABLE I. The $NN$ parameters used for generating the $T = 0$ and $T = 1$ states of $^6$Li. The strengths, $C^n_{\ell\ell'}$, are in units of fm$^{-3}$, while the range parameters, $\beta_{\ell j}$, are in units of fm$^{-1}$.

| Model | Channels | | | | | | | |
|---|---|---|---|---|---|---|---|---|
| | $^3S_1$ | | $^3D_1$ | | $^3S_1$-$^3D_1$ | | $^1S_0$ | |
| | $C^n_{\ell\ell'}$ | $\beta_{\ell j}$ | $C^n_{\ell\ell'}$ | $\beta_{\ell j}$ | $C^n_{\ell\ell'}$ | $\beta_{\ell j}$ | $C^n_{\ell\ell'}$ | $\beta_{\ell j}$ |
| (0%) | -1.0325 | 1.4180 | 0.00 | ... | 0.00 | ... | ... | ... |
| (4%) | -0.6419 | 1.3134 | -1.8320 | 1.5283 | +1.0849 | ... | ... | ... |
| (7%) | -0.3776 | 1.2410 | -7.6301 | 1.9480 | +1.6975 | ... | ... | ... |
| Singlet ($NN$) | ... | ... | ... | ... | ... | ... | -0.3943 | 1.1648 |

TABLE II. The $N\alpha$ parameters used for generating the $T = 0$ and $T = 1$ states of $^6$Li. The strengths, $C^n_{\ell\ell'}$, are in units of fm$^{-3}$ for $S$ wave, and fm$^{-5}$ for $P$ waves. The range parameters, $\beta_{\ell j}$, are in units of fm$^{-1}$.

| Model | Channels | | | | | |
|---|---|---|---|---|---|---|
| | $S_{1/2}$ | | $P_{1/2}$ | | $P_{3/2}$ | |
| | $C^n_{\ell\ell'}$ | $\beta_{\ell j}$ | $C^n_{\ell\ell'}$ | $\beta_{\ell j}$ | $C^n_{\ell\ell'}$ | $\beta_{\ell j}$ |
| $A$ | +1.0519 | 0.7496 | -1.8221 | 1.1770 | -7.9735 | 1.4490 |
| $B$ | +1.0519 | 0.7496 | -3.5188 | 1.3040 | -8.8367 | 1.4810 |

TABLE III. The position of the $P_{1/2}$ and $P_{3/2}$ resonances in the $k$ and $E$ plane for the potentials $A$ and $B$. In calculating the position of the resonances, we have taken $m_p = 939$ MeV, $\hbar c = 197.327$ MeV fm, and the $\alpha$-$N$ reduce mass $\mu = \frac{4}{5}m_p$.

| Model | Channel | $k_R$ | $\varepsilon_R$ |
|---|---|---|---|
| $A$ | $P_{3/2}$ | $0.1667 - 0.0317\,i$ | $0.6944 - 0.2739\,i$ |
| $B$ | $P_{3/2}$ | $0.1766 - 0.0349\,i$ | $0.7767 - 0.3193\,i$ |
| Experiment | $P_{3/2}$ | $0.1766 - 0.03489\,i$ | $0.7778 - 0.3196\,i$ |
| $A$ | $P_{1/2}$ | $0.3172 - 0.1731\,i$ | $1.8312 - 2.8450\,i$ |
| $B$ | $P_{1/2}$ | $0.3109 - 0.1402\,i$ | $1.9958 - 2.2600\,i$ |
| Experiment | $P_{1/2}$ | $0.3111 - 0.1404\,i$ | $1.999 - 2.267\,i$ |

TABLE IV. The $T = 0$ states of $^6$Li. The calculated results are for 0%, 4%, and 7% $D$-state probability for the deuteron, and make use of model $A$ for the $N\alpha$ interactions. All energies and widths are in MeV. The experimental values are from Ajzenberg-Selove [33].

| Levels | Experiment | | 0% | | 4% | | 7% | |
|---|---|---|---|---|---|---|---|---|
| $J^\pi$ | $E$ | $\Gamma$ | $E$ | $\Gamma$ | $E$ | $\Gamma$ | $E$ | $\Gamma$ |
| $1^+$ (g.s.) | -3.70 | 0.00 | -4.45 | 0.00 | -4.06 | 0.00 | -3.82 | 0.00 |
| $3^+$ | -1.515 | 0.024±0.002 | -2.40 | 0.00 | -1.87 | 0.01 | -1.54 | 0.06 |
| $2^+$ | +0.61 | 1.7±0.2 | +0.53 | 1.30 | +0.26 | 1.10 | +0.34 | 1.18 |
| $1^+$ | +1.95 | 1.5±0.2 | +0.90 | 1.43 | +1.05 | 1.72 | +1.05 | 1.78 |

TABLE V. A comparison of the resonance parameters for the $T = 0$, $J^\pi = 2^+$ and $1^+$ states as extracted from the speed analysis and the eigenvalues of the Faddeev kernel. Also included are the experimental results of Refs. [35] and [33]. The results of the calculation are for the $N$-$\alpha$ potential $A$, and the 4% $N$-$N$ potential.

| $J^\pi$ | Experiment | | | | Model | | | |
|---|---|---|---|---|---|---|---|---|
| | Ref. [33] | | Ref. [35] | | Speed | | Eigenvalue | |
| | $E$ | $\Gamma$ | $E$ | $\Gamma$ | $E$ | $\Gamma$ | $E$ | $\Gamma$ |
| $2^+$ | 0.61 | 1.7±0.2 | 0.58 | 1.07 | 0.27 | 1.10 | 0.26 | 1.10 |
| $1^+$ | 1.95 | 1.5±0.2 | 1.66 | 2.62 | 1.08 | 1.40 | 1.05 | 1.72 |

fective range and scattering length. In both $T = 0$ and $T = 1$, for the interaction between the $N$-$\alpha$ pairs, the dominant $P_{3/2}$, $P_{1/2}$, and $S_{1/2}$ components are included. In particular, the $S_{1/2}$ component of the $N$-$\alpha$ interaction is represented by a purely repulsive potential. This component is of utmost importance in incorporating the Pauli exclusion principle at the level of dynamics [28]. As mentioned in the Introduction, it is possible to represent the $N\alpha$ interaction by an attractive potential from which the spurious bound state is excluded by means of a projection method [14, 15]. One of the interesting problems is to see if these different representations of the $S_{1/2}$ component of the $N\alpha$ interaction, by a purely repulsive or an attractive (with projected bound state) potential, can be distinguished by their effects on the calculation of the observables. The electromagnetic form factors do not seem to be effected [28]; however, the binding energy of $^6$He is increased by nearly 40% to give a better agreement with the experimental value, while the binding energy of $^6$Li is shifted away from experiment by ($\lesssim 4\%$) when an attractive (with projected bound state) potential is used for the $S_{1/2}$ component of the $N\alpha$ interaction instead of a purely repulsive one [14]. The question is by no means settled yet. In this work we have opted to use the purely repulsive representation of the $S_{1/2}$ component of the $N\alpha$ potential because it is considerably easier to adopt within the framework of our calculations and we think that our calculations, in particular, would not shed any more light on this problem than the work of Lehman [14]. Moreover, as will be discussed later, more relevant effects might be expected from the inclusion of the excitations of the $\alpha$ particle or the inclusion of the Coulomb interaction.

We assess the sensitivity of our calculations to the role of the $N\alpha$ interaction by using two different parametrizations of the $N\alpha$ potentials labeled by model $A$ and model $B$ (see Table II). In model $A$, the parameters are fitted by the low-energy ($\lesssim 20$ MeV ) $N\alpha$ phase shifts, whereas in model $B$ they are chosen such that the positions and widths of the $P_{3/2}$ and $P_{1/2}$ ($N\alpha$) resonances are reproduced (see the work of Lehman and Gibson for more detail [29]). In Table III we give the position of the $P_{3/2}$ and $P_{1/2}$ poles for the potentials $A$ and $B$. Included also are the position of the $N$-$\alpha$ poles as predicted by the phase shifts [30]. In Figs. 1 and 2 we present the $P_{3/2}$ and $P_{1/2}$ $N\alpha$ phase shifts as given by models $A$ and $B$, respectively, versus the experimental phase shifts (the experimental points are taken from the work of Arndt and co-workers [31]).

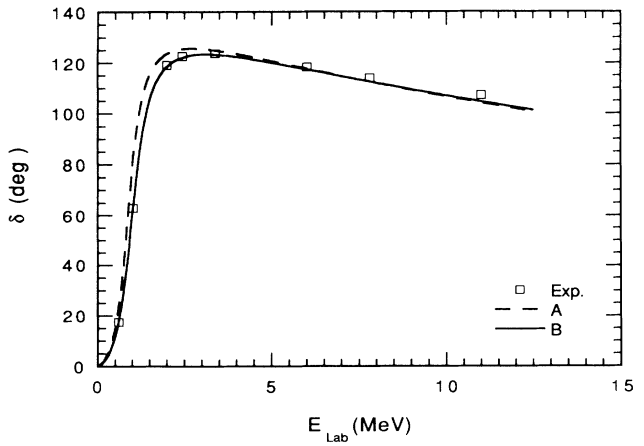


FIG. 1. The $N\alpha$ $P_{3/2}$ phase shifts for model $A$, dashed line, and model $B$, solid line, are presented. The points are the results of the phase analysis of Arndt and co-workers [31].

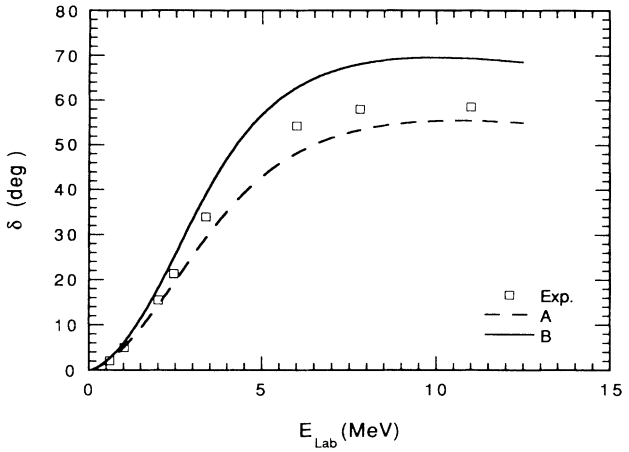


FIG. 2. The $P_{1/2}$ phase shifts for model $A$, dashed line, and model $B$, solid line, are presented. The points are the results of the phase analysis of Arndt and co-workers [31].

## III. NUMERICAL RESULTS

Before we proceed to a discussion of our results for the $A = 6$ system, we should specify the numerical procedure used in the solution of our equations for both the $\alpha$-$d$ scattering amplitude, and the determination of the eigenvalues of the Faddeev kernel. Since we need the method of contour rotation to expose that part of the second and third Riemann sheet of the complex energy plane where resonance poles reside, we have used the same method for the determination of the scattering amplitude as well. In particular, we have chosen the angle of rotation for the scattering amplitude calculations to be one-half the maximum angle of rotation allowed at that energy [32]. With this angle of rotation and 32 point quadrature for the integral equations we get sufficient accuracy to be able to extract the resonance parameters from the "speed" curve.

For the determination of the position of the resonances on the second and third Reimann sheet of the complex energy plane, we have employed the method of Refs. [23, 16]. The singularities of the Faddeev kernel put limitations on the parts of the second and third Riemann sheet of the energy plane that we can access by the method of contour rotation. The most convenient numerical method of analytically continuing the homogeneous Faddeev equation is the rotation of the contour of integration, i.e., $q_\alpha \rightarrow q_\alpha e^{-i\phi}$ and $q_\gamma \rightarrow q_\gamma e^{-i\phi}$. This particular choice for the rotation of the contour of integration renders the moving logarithmic singularities of $Z_{K_\alpha;K_\gamma}(q_\alpha, q_\gamma; E)$ to the imaginary momentum axis [32]. As a result of this,

the only limitation on the rotation of the contour comes from the quasiparticle propagator $\tau_{n_\gamma}$. The two-body unitarity cut in $\tau_{n_\gamma}(E - q_\gamma^2/2\mu_\gamma)$, which gives rise to the three-body unitarity cut in the Faddeev equation, requires that the angle of rotation $\phi$ be greater than $\theta_b$, where

$$\tan 2\theta_b = \frac{E_i}{E_r} , \tag{28}$$

and $E = E_r - iE_i$, $E_i > 0$. This implies that as we analytically continue our equation into the complex energy plane we have to increase the rotation angle of the contour of integration $\phi$. The pole of $\tau_\gamma$ due to the deuteron imposes a similar, but weaker constraint on the rotation angle $\phi$. The most important singularity of $\tau_\gamma$ is the $N$-$\alpha$ resonance pole. This gives rise to a square-root branch point on the second Riemann sheet of the energy plane at $E = \varepsilon_R \equiv \varepsilon_r - i\varepsilon_i$, where $\varepsilon_R$ is the $N$-$\alpha$ resonance energy. In our calculation there are two such branch points corresponding to the $P_{3/2}$ and $P_{1/2}$ resonances in the $N$-$\alpha$ system, and their positions are given in Table III. The $P_{1/2}$ resonance with a half width of more than 2 MeV will not play as important a role as the $P_{3/2}$ resonance. This latter branch point and the corresponding branch cut divide the energy plane into four sections. For energies $E$ such that $E_r < \varepsilon_r$, we can continue our equation in the energy $E$ into the region $E_i > \varepsilon_i$ and $R_r < \varepsilon_r$ with no problem provided $\phi > \theta_b$. On the other hand, for that part of the energy plane with $E_r > \varepsilon_r$ as we continue our equation into the complex energy plane into the region $E_i > \varepsilon_i$, we move into the third Riemann sheet of the energy plane [23]. We now have to make sure that the angle of rotation of the contour of integration, $\phi$, is larger than $\theta_r$, where

$$\tan 2\theta_r = \frac{E_i - \varepsilon_i}{E_r - \varepsilon_r} . \tag{29}$$

Although we can analytically continue our equation beyond these two regions using this method of contour rotation [23], we have not needed that for the present analysis. To get an accuracy of $\approx 0.01$ MeV in the resonance energies, we have had to take $\phi > 1.5\theta_b$ or $\phi > 1.5\theta_r$ depending on the region we are searching, and carry out the final search for the pole with 64 point quadratures

In Table IV we present the calculated $T = 0$ states in $^6$Li for the $N$-$\alpha$ potential $A$, and for the three different potentials with a deuteron $D$-state probability of 0, 4, and 7%. Also included are the "experimental" results as reported by Ajzenberg-Selove [33]. Considering the fact that these $N$-$N$ potentials are simple Yamaguchi potentials that do not have any short-range repulsion and give the wrong sign for the $^3D_1$ phase shifts [34], and that the $S_{1/2}$ $N$-$\alpha$ potential is a one term repulsive separable potential, the overall agreement between the calculated and the experimental spectrum is very good. The two apparent major discrepancies are the width of the $J^\pi = 2^+$, for which the model predicts too small a value, and the position of the $J^\pi = 1^+$ states which is predicted at a lower energy than observed experimentally. Both of these states are close to the square-root branch cut due to the production of a resonant $A = 5$ system in the $P_{3/2}$ channel. We note at this stage that the square root branch point at $E = 0.78 - 0.32i$ MeV is closer to the physical region than either of the $1^+$ or $2^+$ states. This square root branch cut is not included in any analysis of the $\alpha$-$d$ data to extract resonance parameters based on speed analysis. It is also not included in the recent energy-dependent Padè analysis of the $d$-$\alpha$ scattering data [35]. This may suggest that there might be a problem in the analysis of the experimental data in terms of the simple idea that the resonance can be represented by a Breit-Wigner form, i.e., a simple pole, and therefore does not include the effect of the square-root branch point.

To examine the role the square-root branch point plays in the analysis of the data, we have calculated the $\alpha$-$d$ amplitude in both the $J^\pi = 1^+$ and $2^+$ channels as a function of the energy. We then used the phase shifts in the $^3D_2$ and $^3D_1$ channels to calculate the speed in this channel. In Table V we compare the results of the determination of the resonance parameters using the speed analysis and the search for the pole in the complex plane by calculating the eigenvalues of the Faddeev kernel. Also included are the experimental results from the tabulation of Ajzenberg-Selove [33] and the more recent energy-dependent analysis of Krasnopol'sky *et al.* [35]. By comparing the speed and eigenvalue method we observe that for the $2^+$, the two methods give the same results within the accuracy of the methods. However, for the $1^+$, the width as predicted by the speed analysis is less than predicted from the position of the pole. This could be due to the fact that the $1^+$ resonance pole is on the third Riemann sheet further from the real axis than

TABLE VI. The $T = 0$ states of $^6$Li. Comparison between different $N\alpha$ interactions. The $NN$ interaction is taken to have 0% $D$-state probability. All energies and widths are in MeV.

| Levels | Experiment | | Model $A$ | | Model $B$ | |
|---|---|---|---|---|---|---|
| $J^\pi$ | $E$ | $\Gamma$ | $E$ | $\Gamma$ | $E$ | $\Gamma$ |
| $1^+$ (g.s.) | -3.70[a] | 0.00[a] | -4.45 | 0.00 | -4.75 | 0.00 |
| $3^+$ | -1.515[a] | 0.024±0.002[a] | -2.40 | 0.00 | -2.25 | 0.00 |
| $2^+$ | +0.58[b] | 1.07[b] | +0.53 | 1.30 | +0.15 | 0.80 |
| $1^+$ | +1.59±0.1[c] | 1.9±0.1[c] | +0.90 | 1.43 | +0.85 | 1.06 |

[a]The experimental results of Ref. [33].
[b]The experimental results of Ref. [35].
[c]The experimental results of Ref. [36].

TABLE VII. The $T = 1$ states of $^6$Li for the two models of the $N\alpha$ interaction. All energies and widths are in MeV. The experimental values are from Ajzenberg-Selove [33].

| Levels | Experiment | | Model $A$ | | Model $B$ | |
|---|---|---|---|---|---|---|
| $J^\pi$ | $E$ | $\Gamma$ | $E$ | $\Gamma$ | $E$ | $\Gamma$ |
| $0^+$ | -0.137 | $(8.2\pm 0.2)\times 10^{-6}$ | -0.56 | 0.00 | -0.45 | 0.00 |
| $2^+$ | +1.67 | 0.540±0.020 | +0.95 | 0.30 | +1.08 | 0.35 |

the square-root branch point. As a result, the speed analysis does not see the pole on its own. This situation does not arise for the $2^+$ since that pole is, in this model, at a much lower energy than the branch point. A comparison of two analyses of the experimental data indicate a considerable discrepancy, particularly in the width determination. For the $2^+$, the results of Krasnopol'sky *et al.* include more recent data and the analysis was done in the region of this resonance. To that extent their results might be more reliable. On the other hand, for the $1^+$ resonance, Krasnopol'sky *et al.* extrapolated their $S$ matrix from lower energy to the region of the $1^+$ resonance. As a result, their determination of the width is substantially larger than the results of Jenny *et al.* [36] which give a width of 1.9 MeV. With the above observation regarding the experimental data, the main discrepancy between our model and experiment is the position of the $1^+$ resonance. Considering the simplicity of our two-body input, there is scope for improvement.

We now turn to the sensitivity of our results to the $\alpha$-$N$ input interaction in the $P_{3/2}$ and $P_{1/2}$ channels. In Table VI we compare the results for the $N$-$\alpha$ potential $A$ which gives an optimum fit to the $P$-wave phase shifts, and potential $B$ whose parameters were adjusted to fit the position of the $P_{3/2}$ and $P_{1/2}$ resonance poles. We have also included the experimental results. In the case of the ground state and $3^+$ state, we have given the results of Ajzenberg-Selove [33], while for the $2^+$ state we have given the results of Krasnopol'sky *et al.* [35], who fitted the data in the region of this resonance with Padè approximation for the $S$ matrix. Finally, for the $1^+$ we give the results of Jenny *et al.* [36]. Here we find that the ground state and first excited state are not very sensitive to the choice of the $P$-wave $N$-$\alpha$ interaction, but the $2^+$ and $1^+$ states are very sensitive, suggesting that one might get a better fit to the experimental data by a better choice of the $P$-wave interaction.

Finally in Table VII we present our results for the $T = 1$ states, which cannot be observed in $\alpha$-$d$ scattering, for both $N$-$\alpha$ potentials. Here the results are not very sensitive to the choice of the two-body input, and although in absolute value the agreement with experiment is not very good, the spacing between the levels is in reasonable agreement with experiment. One expects a shift upwards in the spectrum if one uses a $^1S_0$ $N$-$N$ potential that has short-range repulsion. In addition, we may have to improve on the $S_{1/2}$ $N$-$\alpha$ interaction, if we are to get a more realistic model for the $A = 6$ nuclei.

## IV. CONCLUSIONS

In the present investigation we have made use of a three-body model for the description of the low-lying states of the $A = 6$ nuclei. In particular, we have used the model based on the Faddeev equations with separable potentials for the description of the $T = 0$ and 1 bound states and low energy resonances of the $\alpha$-$N$-$N$ system. Since both the bound and resonance states are eigenstates of the Hamiltonian when analytically continued to the second and third Riemann sheet of the energy plane, we use the homogeneous Faddeev equations for both classes of states. We find that with the simplest of separable potentials, for both the $N$-$N$ and $N$-$\alpha$ interactions, we get a reasonable description of low-energy $T = 0$ and 1 spectra of the $A = 6$ nuclei. The wave functions for these states can also be determined by calculating the eigenvectors of the Faddeev kernel at the resonance energies. Finally, by comparing the results of the speed analysis with the position of the resonance pole, we may conclude that for resonances close to the square-root branch point resulting from the production of a resonant subsystem the speed analysis might be misleading.

The agreement with experiment can be improved by replacing the present $N$-$N$ interaction by a separable approximation to any of a number of more realistic potentials. Furthermore, since we are only considering the homogeneous Faddeev equations, we can include the Coulomb potential for the resonance state as suggested for the bound state by Lehman *et al.* [37]. This work is presently in progress.

## ACKNOWLEDGMENTS

The authors would like to thank the Australian Research Council for their financial support during the course of this work.

[1] P. E. Shanley, Phys. Rev. **187**, 1328 (1969).
[2] Y. Koike, Prog. Theor. Phys. **55**, 2016 (1976).
[3] Y. Koike, Prog. Theor. Phys. **59**, 87 (1978).
[4] Y. Koike, Nucl. Phys. **A301**, 411 (1978).
[5] Y. Koike, Nucl. Phys. **A337**, 23 (1980).
[6] D. R. Lehman and M. Rajan, Phys. Rev. C **25**, 2743 (1982); W. C. Parke and D. R. Lehman, *ibid.* **29**, 2319 (1984).
[7] C. T. Christou, C. J. Seftor, W. J. Briscoe, W. C. Parke, and D. R. Lehman, Phys. Rev. C **31**, 250 (1985); R. Ent, H. P. Blok, J. F. A. van Heinen, G. van der Steenhoven, J. F. J. van den Brand, J. W. A. den Herder, E. Jans,

P. H. M. Keizer, L. Lapikas, E. N. M. Quint, P. K. A. de-Witt Huberts, B. L. Berman, W. J. Briscoe, C. T. Christou, D. R. Lehman, B. E. Norum, and A. Saha, Phys. Rev. Lett. **57**, 2367 (1986).
[8] M. Rai, D. R. Lehman, and A. Ghovanlou, Phys. Lett. **59B**, 327 (1975).
[9] C. T. Christou, D. R. Lehman, and W. C. Parke, Phys. Rev. C **37**, 445 (1988); **37**, 458 (1988).
[10] W. C. Parke, A. Ghovanlou, C. T. Noguchi, M. Rajan, and D. R. Lehman, Phys. Lett. **74B**, 158 (1978).
[11] Y. Matsui, Phys. Rev. C **22**, 2591 (1980).
[12] D. R. Lehman, M. Rai, and A. Ghovanlou, Phys. Rev. C **17**, 744 (1978).
[13] A. Ghovanlou and D. R. Lehman, Phys. Rev. C **9**, 1730 (1974).
[14] D. R. Lehman, Phys. Rev. C **25**, 3146 (1982).
[15] V. M. Krasnopol'skii and V. I. Kukulin, Yad. Fiz. **20**, 883 (1974) [Sov. J. Nucl. Phys. **20**, 470 (1975)].
[16] B. C. Pearce and I. R. Afnan, Phys. Rev. C **30**, 2022 (1984).
[17] I. R. Afnan and B. C. Pearce, Phys. Rev. C **31**, 986 (1985).
[18] Arthur H. Rosenfeld *et al.*, Rev. Mod. Phys. **39**, 1 (1967).
[19] J. Aguilar and J. M. Combes, Commun. Math. Phys. **22**, 269 (1971).
[20] E. Balslev and J. M. Combes, Commun. Math. Phys. **22**, 280 (1971).
[21] B. Simon, Ann. Math. **97**, 247 (1973).
[22] C. Lovelace, in *Strong Interaction and High Energy Physics*, Scottish University Summer School, edited by R. G. Moorhouse (unpublished).
[23] I. R. Afnan, Aust. J. Phys. **44** (1991).
[24] E. O. Alt, P. Grassberger, and W. Sandhas, Nucl. Phys. **B2**, 167 (1967).
[25] I. R. Afnan and A. W. Thomas, in *Modern Three-Hadron Physics*, edited by A. W. Thomas (Springer, Berlin, 1977), Chap. 1.
[26] I. R. Afnan and A. W. Thomas, Phys. Rev. C **10**, 109 (1974).
[27] I. R. Afnan and B. F. Gibson, Phys. Rev. C **41**, 2787 (1990).
[28] A. Eskandarian, D. R. Lehman, and W. C. Parke, Phys. Rev. C **38**, 2341 (1988); **39**, 1685 (1989).
[29] D. R. Lehman and B. F. Gibson, Phys. Rev. C **16**, 1275 (1977).
[30] M. U. Ahmed and P. E. Shanley, Phys. Rev. Lett. **36**, 25 (1976).
[31] R. A. Arndt, Dale D. Long, and L. David Roper, Nucl. Phys. **A209**, 429 (1973); R. A. Arndt and L. David Roper, *ibid.* **A209**, 447 (1973).
[32] A. T. Stelbovics, Nucl. Phys. **A288**, 461 (1977).
[33] F. Ajzenberg-Selove, Nucl. Phys. **A490**, 1 (1988).
[34] I. R. Afnan and J. M. Read, Aust. J. Phys. **26**, 725 (1973).
[35] V. M. Krasnopo'sky, V. I. Kukulin, E. V. Kuznetsova, J. Horàček, and N. M. Queen, Phys. Rev. C **43**, 822 (1991).
[36] B. Jenny, W. Grübler, V. König, P. A. Schmelzbach, and C. Schweizer, Nucl. Phys. **A397**, 61 (1983).
[37] D. R. Lehman, A. Eskandarian, B. F. Gibson, and L. C. Maximon, Phys. Rev. C **29**, 1450 (1984).